



Cadmium(II) and zinc(II) coordination polymers with mixed building blocks of benzenedicarboxyl and 2,5-bipyridyl-1,3,4-oxadiazole: Syntheses, crystal structures, and properties

Jing Chen, Shang-Yuan Liu, Cheng-Peng Li*

College of Chemistry, Tianjin Key Laboratory of Structure and Performance for Functional Molecule, Tianjin Normal University, Tianjin 300387, PR China

ARTICLE INFO

Article history:

Received 5 January 2011

Received in revised form 10 August 2011

Accepted 31 August 2011

Available online 8 September 2011

Keywords:

Coordination polymer

Crystal structure

Benzenedicarboxylic acid

2,5-Bipyridyl-1,3,4-oxadiazole

Secondary interaction

ABSTRACT

Three Cd(II) and Zn(II) coordination polymers, including $\{[\text{Cd}(3\text{-bpo})(\text{mip})(\text{H}_2\text{O})](\text{H}_2\text{O})_2\}_n$ (**1**), $\{[\text{Cd}(4\text{-bpo})(\text{hip})(\text{H}_2\text{O})](\text{H}_2\text{O})_4\}_n$ (**2**), and $\{[\text{Zn}(4\text{-bpo})(\text{tp})](\text{CH}_3\text{OH})\}_n$ (**3**) were synthesized from the reactions of Cd^{II} or Zn^{II} nitrate with mixed organic ligands [3-bpo = 2,5-bis(3-pyridyl)-1,3,4-oxadiazole, H₂mip = 5-methylisophthalic acid, 4-bpo = 2,5-bis(4-pyridyl)-1,3,4-oxadiazole, H₂hip = 5-hydroxyisophthalic acid, H₂tp = terephthalic acid] under the similar layered diffusion condition. The resulting crystalline materials **1–3** were characterized by IR, microanalysis, powder X-ray diffraction (PXRD) techniques. Single-crystal X-ray diffraction indicates a 1-D tubular motif for **1**, a 1-D dual-track array for **2**, and a 2-D grid-like pattern for **3**, constructed via different metal–ligand coordination contacts. Higher-dimensional supramolecular architectures are further assembled in **1–3** via H-bonding and aromatic stacking interactions. In addition, thermal stability and fluorescence of these polymeric complexes were also investigated and discussed.

© 2011 Elsevier B.V. All rights reserved.

1. Introduction

The design and preparation of coordination supramolecular chemistry has become an attractive research field in recent years, producing a large number of coordination complexes which are generally assembled from fine-tuning molecular building tectons with unambiguous intermolecular interactions [1–14]. In particular, their ease of structural regulation and potential physicochemical properties, such as guest absorption, optics, ion exchange, chirality, catalysis, magnetism, etc., provide good explanations to structure–function relationship thereof [15–26]. Construction of such supramolecular systems can be achieved by the combination of metal ions and organic ligands in a well-rounded manner [27–31].

As for the d¹⁰ metal elements, especially for Cd and Zn, they prefer the +2 oxidation state in most of their complexes, and commonly possess the coordination numbers from 4 to 7 and the corresponding geometries, which can be utilized to prepare multi-form metallosupramolecular complexes [32]. On the other hand, to meet the requirement of metal–ligand binding preference and the energetic consideration of overall crystal packing, mixed-ligand assembling strategy may be the most effective approach. A variety of organic ligands, especially for polycarboxylate and polypyridyl

types, have been generally regarded as the most familiar and reliable candidates to construct the desired coordination architectures in recent years [33–35]. In this direction, as a continuation of our research, we selected the modified bent dipyridyl ligands, namely, 2,5-bis(3-pyridyl)-1,3,4-oxadiazole (3-bpo) and its 4-pyridyl analog (4-bpo), as well as different benzenedicarboxylic acids [5-methylisophthalic acid (H₂mip), 5-hydroxyisophthalic acid (H₂hip), and terephthalic acid (H₂tp)] as building tectons, to assemble with Cd(II) or Zn(II) nitrates under ambient conditions. First, the paired analog bpo ligands can be viewed as not only the extension of traditionally employed 4,4'-bipyridine ligand, but also the modification types with longer and bent spacers, flexible conformations, as well as various coordination modes [36]. Second, these benzenedicarboxylic isomers contain two carboxyl groups at distinct positions, which may engender significant spatial effect and thus influence the structural assembly with multiform coordination fashions. Third, the cooperation of bpo and benzenedicarboxylic counterparts can produce directional conformation of network structures via coordination bonds and also noncovalent cooperative forces, such as hydrogen bonding and/or aromatic stacking. In this context, three novel coordination polymers, $\{[\text{Cd}(3\text{-bpo})(\text{mip})(\text{H}_2\text{O})](\text{H}_2\text{O})_2\}_n$ (**1**), $\{[\text{Cd}(4\text{-bpo})(\text{hip})(\text{H}_2\text{O})](\text{H}_2\text{O})_4\}_n$ (**2**), and $\{[\text{Zn}(4\text{-bpo})(\text{tp})](\text{CH}_3\text{OH})\}_n$ (**3**) are prepared, which display different 1-D and 2-D coordination motifs and supramolecular networks via secondary interactions. In addition, their thermal stability and fluorescence were also investigated.

* Corresponding author.

E-mail address: tjnulicp@gmail.com (C.-P. Li).

2. Experimental

2.1. Materials and general methods

With the exception of the ligands 3-bpo and 4-bpo, which were synthesized according to the reported procedures [37], all reagents and solvents for synthesis and analysis were commercially available and used as received. Fourier transform (FT) IR spectra (KBr pellets) were taken on an AVATAR-370 (Nicolet) spectrometer. Elemental analyses of C, H, and N were performed on a CE-440 (Leemanlabs) analyzer. Thermogravimetric analysis (TGA) curves were carried out on a NETZSCH TG209 (Siemens) thermal analyzer in the range of 25–600 °C at a heating rate of 10 °C/min under N₂ atmosphere. Powder X-ray diffraction (PXRD) patterns were recorded on a Rigaku D/Max-2500 diffractometer at 40 kV and 100 mA for a Cu-target tube ($\lambda = 1.5406 \text{ \AA}$). The calculated PXRD patterns were obtained from the single-crystal diffraction data using the PLATON software. Fluorescence spectra of the solid samples were measured on a Cary Eclipse spectrofluorimeter (Varian) at room temperature.

2.2. Synthesis of complexes 1–3

2.2.1. $\{[\text{Cd}(3\text{-bpo})(\text{mip})(\text{H}_2\text{O})](\text{H}_2\text{O})_2\}_n$ (**1**)

A mixture containing 3-bpo (11.2 mg, 0.05 mmol) and H₂mip (9.0 mg, 0.05 mmol) in CH₃OH (5 mL) was layered onto an aqueous solution (5 mL) of Cd(NO₃)₂·8H₂O (30.8 mg, 0.1 mmol). Colorless block single crystals of **1** were found on the wall of test tube after ca. a month and collected in a yield of 56% (15.8 mg, based on 3-bpo). *Anal.* Calc. for C₂₁H₂₀CdN₄O₈ (**1**): C, 44.34; H, 3.54; N, 9.85. Found: C, 44.55; H, 3.69; N, 10.03%. IR (cm⁻¹): 3447b, 1605s, 1549w, 1428s, 1331m, 1261vs, 1116b, 1031vs, 960w, 823s, 731m, 689m, 634m, 459m.

2.2.2. $\{[\text{Cd}(4\text{-bpo})(\text{hip})(\text{H}_2\text{O})](\text{H}_2\text{O})_4\}_n$ (**2**)

A mixed solution of 4-bpo (11.2 mg, 0.05 mmol) and H₂hip (9.1 mg, 0.05 mmol) in CH₃OH (5 mL) was layered onto an aqueous solution (5 mL) of Cd(NO₃)₂·8H₂O (30.8 mg, 0.1 mmol). Colorless block single crystals of **2** were observed on the wall of test tube after ca. 1 week and collected in 55% yield (16.8 mg, based on 4-bpo). *Anal.* Calc. for C₂₀H₂₂CdN₄O₁₁ (**2**): C, 39.59; H, 3.65; N, 9.23. Found: C, 39.86; H, 3.89; N, 9.18%. IR (cm⁻¹): 3434b, 1618w, 1562vs, 1386vs, 1275m, 1219s, 1110w, 1002s, 785s, 729s, 585m.

2.2.3. $\{[\text{Zn}(4\text{-bpo})(\text{tp})](\text{CH}_3\text{OH})\}_n$ (**3**)

A mixture of 4-bpo (11.2 mg, 0.05 mmol) and H₂tp (8.3 mg, 0.05 mmol) in CH₃OH (5 mL) was layered onto a water solution (5 mL) of Zn(NO₃)₂·6H₂O (29.7 mg, 0.1 mmol). Yellow block single crystals of **3** were observed on the wall of test tube after ca. one week and collected in a yield of 71% (17.2 mg, based on 4-bpo). *Anal.* Calc. for C₂₁H₁₆ZnN₄O₆ (**3**): C, 51.92; H, 3.32; N, 11.53. Found: C, 52.04; H, 3.29; N, 11.65%. IR (cm⁻¹): 3242b, 1692w, 1617m, 1588s, 1541vs, 1493s, 1422s, 1385vs, 1286s, 1058w, 1011s, 840s, 787s, 736s, 536w, 497w.

2.3. X-ray single crystal diffraction

Single-crystal X-ray diffraction data for complexes **1–3** were collected on a Bruker Apex II CCD diffractometer at room temperature with Mo K α radiation ($\lambda = 0.71073 \text{ \AA}$). There was no evidence of crystal decay during data collection. Generally, a semi-empirical absorption correction (SADABS) was applied and the program SAINT was used for integration of the diffraction profiles [38]. The structures were solved by direct methods using the SHELXS program of the SHELXTL package and refined with SHELXL [39]. The final refinements were performed by full-matrix least-squares methods on F^2 with anisotropic thermal parameters for all non-H atoms. Hydrogen atoms attached to carbon were generated geometrically, and those of hydroxyl of hip, and lattice methanol or water were first located in difference Fourier syntheses and then treated as riding. Isotropic displacement parameters of H were derived from their parent atoms. As for **1**, both lattice aqua molecules of O8 and O9 are disordered over two sites, with each part possessing the quarter site-occupancy. All H atoms of the lattice water molecules cannot be located. For **2**, O10 was treated using a disordered model over two sites, with the partial site-occupancies of 0.20/0.80, the H atoms of which were also not located. A summary of the crystallographic data of **1–3** are listed in Table 1. Selected bond parameters and H-bonding geometries are shown in Tables S1 and S2 (in Supplementary material).

3. Results and discussion

3.1. Synthesis and general characterization

In the syntheses of complexes **1–3**, a layer-separation diffusion approach in water-methanol readily facilitates the slow growth of

Table 1
Crystallographic data and structural refinement summary for complexes 1–3.

| Compound reference | 1 | 2 | 3 |
|--|---|--|---|
| Chemical formula | C ₂₁ H ₂₀ CdN ₄ O ₈ | C ₂₀ H ₂₂ CdN ₄ O ₁₁ | C ₂₁ H ₁₆ ZnN ₄ O ₆ |
| Formula mass | 568.81 | 606.82 | 485.77 |
| Crystal system | monoclinic | triclinic | monoclinic |
| <i>a</i> (Å) | 9.820(2) | 7.7332(15) | 9.5268(10) |
| <i>b</i> (Å) | 18.193(4) | 9.7404(18) | 15.3121(16) |
| <i>c</i> (Å) | 25.679(6) | 17.238(3) | 15.5250(12) |
| α (°) | 90.00 | 91.833(3) | 90.00 |
| β (°) | 90.132(4) | 97.011(3) | 117.816(5) |
| γ (°) | 90.00 | 109.782(3) | 90.00 |
| Unit cell volume (Å ³) | 4587.7(17) | 1208.9(4) | 2003.0(3) |
| Temperature (K) | 296(2) | 296(2) | 296(2) |
| Space group | C2/c | P $\bar{1}$ | P2 ₁ /c |
| Number of formula units per unit cell (<i>Z</i>) | 8 | 2 | 4 |
| Absorption coefficient (μ/mm^{-1}) | 1.007 | 0.969 | 1.275 |
| Number of reflections measured | 11633 | 6250 | 10197 |
| Number of independent reflections | 4065 | 4249 | 3546 |
| R_{int} | 0.0173 | 0.0111 | 0.0180 |
| Final R_1 values ($I > 2\sigma(I)$) | 0.0257 | 0.0245 | 0.0270 |
| Final wR (F^2) values ($I > 2\sigma(I)$) | 0.0726 | 0.0650 | 0.0707 |
| Final R_1 values (all data) | 0.0299 | 0.0271 | 0.0338 |
| Final wR (F^2) values (all data) | 0.0748 | 0.0668 | 0.0752 |
| Goodness of fit (GOF) on F^2 | 1.082 | 1.055 | 1.037 |

well-shaped single crystals suitable for X-ray single-crystal diffraction. Instead of this, only a mass of microcrystalline solids can be obtained from the direct metal–ligand assemblies in the homogeneous solutions. Although the metal/dicarboxyl/bpo ratio of 2:1:1 was used for the starting materials in each assembling case, the resulting complexes all possess the equivalent metal/dicarboxyl/bpo ratio, as confirmed by elemental analysis and single crystal X-ray diffraction. As for the IR spectra of **1–3**, the broad bands centered at *ca.* 3400 cm⁻¹ reveal the O–H characteristic stretching vibrations of water, hydroxyl, or methanol. No obvious adsorption peak at *ca.* 1700 cm⁻¹ is observed, indicating a complete deprotonation of the dicarboxyl ligands in all complexes. Correspondingly, the peaks at 1562–1605 and 1385–1428 cm⁻¹ can be properly assigned to the antisymmetric and symmetric stretching vibrations of the deprotonated carboxylate groups. The phase purity of the bulk crystalline sample was also confirmed by PXRD technique for each complex, showing a good agreement of the experimental and calculated patterns (see Fig. S1 in Supplementary material).

3.2. Structural analysis of **1–3**

3.2.1. $\{[Cd(3\text{-bpo})(mip)(H_2O)](H_2O)_2\}_n$ (**1**)

Single-crystal X-ray diffraction indicates that complex **1** shows a 1-D polymeric tubular motif. The asymmetric unit of **1** is composed of one Cd(II) ion, one mip dianion, one 3-bpo, as well as one coordinated and two lattice water molecules. As depicted in Fig. 1a, the coordination sphere of each Cd(II) center can be portrayed as a distorted pentagonal–bipyramid, in which the metal ion is coordinated by five O atoms from two mip and one water ligands in the equatorial plane, and paired *trans*-pyridyl N donors of 3-bpo located at the axial positions. The carboxylates of mip both take the chelating coordination fashion. In this 1-D polymeric motif, two adjacent Cd(II) centers (Cd···Cd = 8.223(1) Å) are doubly bridged by a pair of 3-bpo ligands to feature a bimetallic macrocyclic unit. The dimeric units are further interconnected by paired mip ligands to produce a tubular array (see Fig. 1b), in which the lattice water molecules of O9 are located and interact with the carboxylates of mip (O9···O4 = 2.553(1) Å). In addition, the coordinated water molecules of O6 are involved in the intrachain O6–H6A···O3 and interchain O6–H6A···N3 hydrogen bonding (see Table S2 for details), which extend the 1-D arrays into a 2-D supramolecular layered framework (see Fig. 1c). Moreover, the rich aromatic 3-bpo systems facilitate multiple aromatic stacking contacts between the oxadiazole and pyridyl rings, with the centroid-to-centroid distances and the dihedral angles between the corresponding groups of 3.556–3.752 Å and 2.0–5.6°. Further investigation of the crystal packing indicates that these parallel H-bonding 2-D layers are arranged in an offset mode, without any significant secondary interactions between them.

3.2.2. $\{[Cd(4\text{-bpo})(hip)(H_2O)](H_2O)_4\}_n$ (**2**)

Complex **2** displays a polymeric dual-track array that is completely different from that of **1**. In this structure, the asymmetric unit consists of one Cd^{II}, one 4-bpo, one hip, as well as one coordinated and four lattice water molecules. Each Cd^{II} ion is surrounded by four carboxylate O atoms from a pair of hip and one pyridyl N donor to constitute the equatorial plane, as well as two water ligands in the axial positions (see Fig. 2a). Similar to that of **1**, the local coordination geometry of Cd^{II} can also be described as a distorted pentagonal–bipyramid, although they have different coordination donors (CdN₂O₅ for **1** and CdNO₆ for **2**). For each hip ligand, the two carboxylate groups take the chelating and μ -O,O- η -O,O' bridging coordination modes. As a result, the adjacent Cd^{II} centers are connected by the μ_3 -hip linkers to generate a 1-D dual-track array, with the unidentate 4-bpo ligands outspread at both sides (see Fig. 2b). Interestingly, the familiar dimeric [Cd₂(μ_2 -COO⁻)₂] units

are observed in this case, with the separation of Cd···Cd thereof being 4.070(1) Å. A side view from the [010] direction shows that the terminal pyridyl rings of extended 4-bpo pendants engender the H-bonding interactions with the hydroxyl groups of hip (O6–H6···N4), resulting in a 2-D H-bonding layer (see Fig. 2c). Furthermore, such 2-D patterns are linked by O7–H7A···O3 bonds between the aqua ligands and carboxylates of hip to form a 3-D supramolecular network (see Fig. 2d). In addition, there also exist O–H···O and O–H···N bonds between the lattice water molecules and the 3-D network (see Table S2 for details), as well as multiple aromatic stacking contacts between the aromatic planes of 4-bpo and hip ligands.

3.2.3. $\{[Zn(4\text{-bpo})(tp)](CH_3OH)\}_n$ (**3**)

The 2-D layered network of **3** is composed of the familiar paddle-wheel [Zn₂(COO)₄] building units, in which the Zn^{II} ion has a distorted square–pyramidal coordination sphere, being completed by four carboxylate O atoms from four distinct tp and one pyridyl N donor (see Fig. 3a). Within this bimetallic unit, the Zn···Zn distance is 2.921(1) Å and each carboxylate group in tp adopts the μ -O,O' bridging mode. Along the *bc* plane, the dimeric subunits are extended by the tp ligands to form an infinite 2-D layered net with the dimension of 10.903(1) × 10.903(1) Å² (see Fig. 3b). Moreover, the lattice methanol molecules are attached to the 2-D layer via O6–H6A···N4 bonds (see Table S2 for details). Notably, the 2-D motif is decorated with the unidentate 4-bpo ligands as side arms at both sides. Of further interest, these long prominent 4-bpo arms, with a length of 9.947(3) Å between the two pyridyl N donors, penetrate into the void grids of the adjacent 2-D layers to form a novel 3-D polythreading supramolecular architecture with finite components (see Fig. 3c) [40]. The adjacent layers take a parallel stacking, in which each mesh of a layer is occupied oppositely by two 4-bpo lateral pendants coming from different layers, with the presence of π ··· π stacking interactions between their pyridyl rings (centroid-to-centroid distance: 3.658 Å and dihedral angle: 7.3°). In addition, the phenyl groups of tp from the in-between layer are also involved in π ··· π stacking interactions with the oxadiazole rings of 4-bpo from the adjacent layers, with the centroid-to-centroid distance and the dihedral angle of 3.613 Å and 3.6°, which further stabilize the 3-D supramolecular network.

3.3. Structural diversity of coordination polymers **1–3**

Complexes **1–3** were obtained under similar synthetic conditions and their structural differences can be exclusively attributed to different metal ions and mixed-ligands used in the assembled processes. A comparison of these structures reveals that the Cd^{II} and Zn^{II} ions tend to adopt the pentagonal–bipyramidal and square–pyramidal coordination geometries, respectively. In **1–3**, the 3-bpo ligand exhibits the bridging function, whereas 4-bpo behaves as terminal coordination, constructing the resulting 1-D and 2-D coordination patterns. As for **1**, in favor of the bridging role of 3-bpo and mip “struts”, a 1-D tubular motif can be achieved and rich aromatic packing interactions are found between the 3-bpo and mip ligands. In **2**, the polymeric 1-D dual-track array is constituted by the hip “struts” and 4-bpo side arms, and O–H···N bonds between the 4-bpo and hip from different chains further extend the resultant supramolecular structure. With regard to **3**, the tp ligands extend the paddle-wheel dinuclear units along two directions to result in a 2-D grid-like framework with the 4-bpo as pendent arms. Moreover, the rich pyridyl and phenyl rings in the mixed-ligand system facilitate the formation of aromatic stacking interactions to stabilize the 3-D supramolecular network.

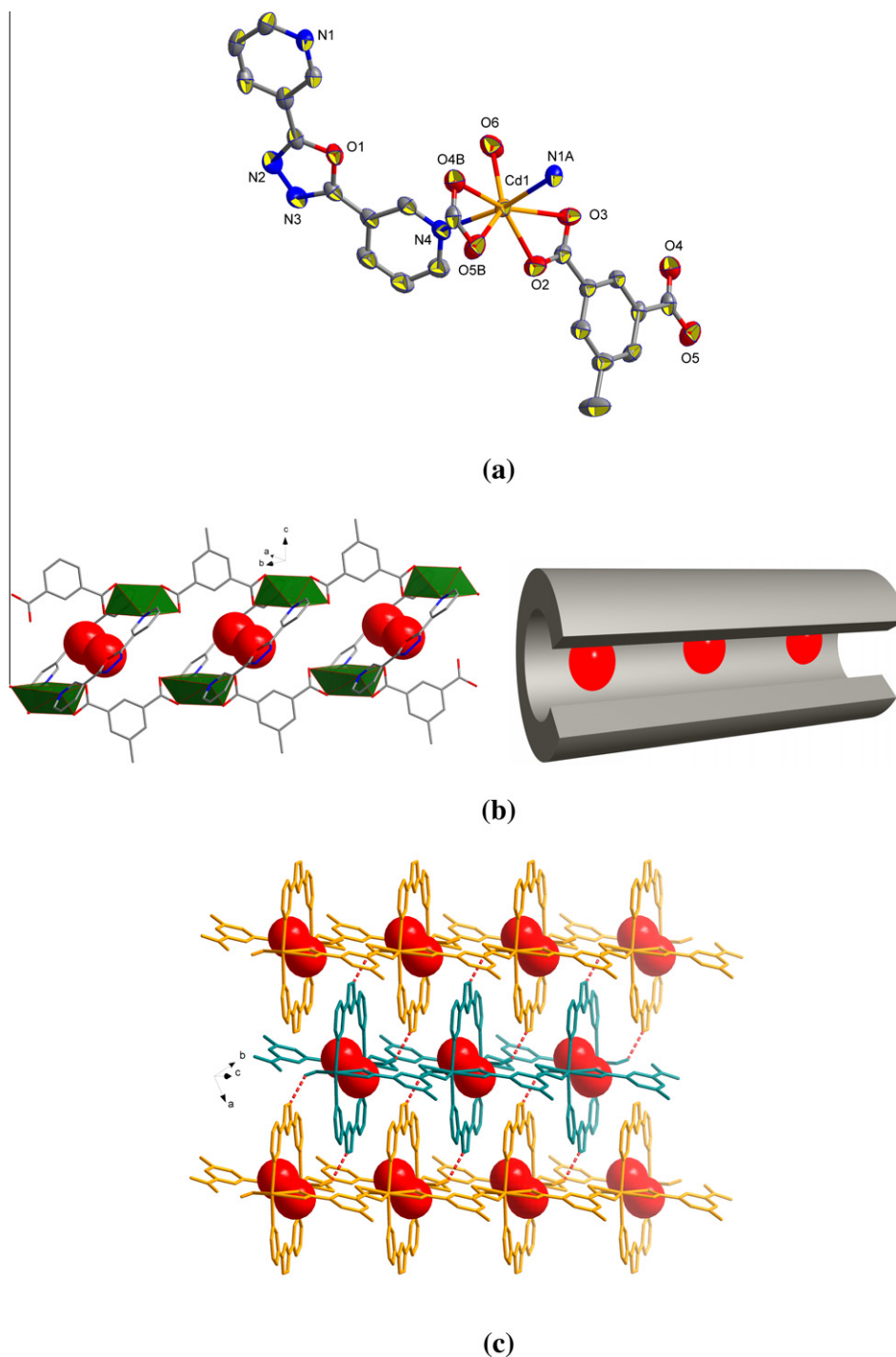


Fig. 1. Crystal structure of **1**. (a) A local view showing the coordination geometry of Cd^{II} (symmetry codes: $A = -x + 1, -y, -z + 1, B = x - 1/2, y + 1/2, z$). (b) Views of the 1-D tubular coordination motif with the accommodation of lattice water molecules (shown as red balls). (c) 2-D H-bonding layer constructed via interchain O–H...O interactions (shown as red dashed lines). (For interpretation of the references to color in this figure legend, the reader is referred to the web version of this article.)

3.4. Thermal stability of complexes **1–3**

The thermal stability of **1–3** was studied by TGA experiments (see Fig. S2 for TGA curves). Complex **1** is thermally stable until heating to *ca.* 220 °C, upon which a very sharp weight loss is observed and ends at *ca.* 360 °C. The loss of lattice water moiety is not observed, which may be concomitant with the collapse of the coordination framework [27,33]. Further heating to 600 °C indicates no obvious weight loss, and the final solid holds a weight of 23.31% of the total sample, which seems to be CdO (calculated:

22.58%). In the TGA curve of **2**, the first weight loss of 11.39% in the range of 35–80 °C reveals the expulsion of four lattice water molecules (calculated: 11.86%). Then, the residual framework keeps stable until 370 °C with two consecutive weight losses that stop at 520 °C. Further heating to 600 °C indicates no weight loss and the remaining solid (20.79% of the total sample) appears to be CdO (calculated: 21.09%). With regard to **3**, the first weight loss of 6.39% in the region of 100–146 °C can be ascribed to the release of lattice methanol molecule (calculated: 6.59%). After that, the residue suffers a series of consecutive weight losses, which end

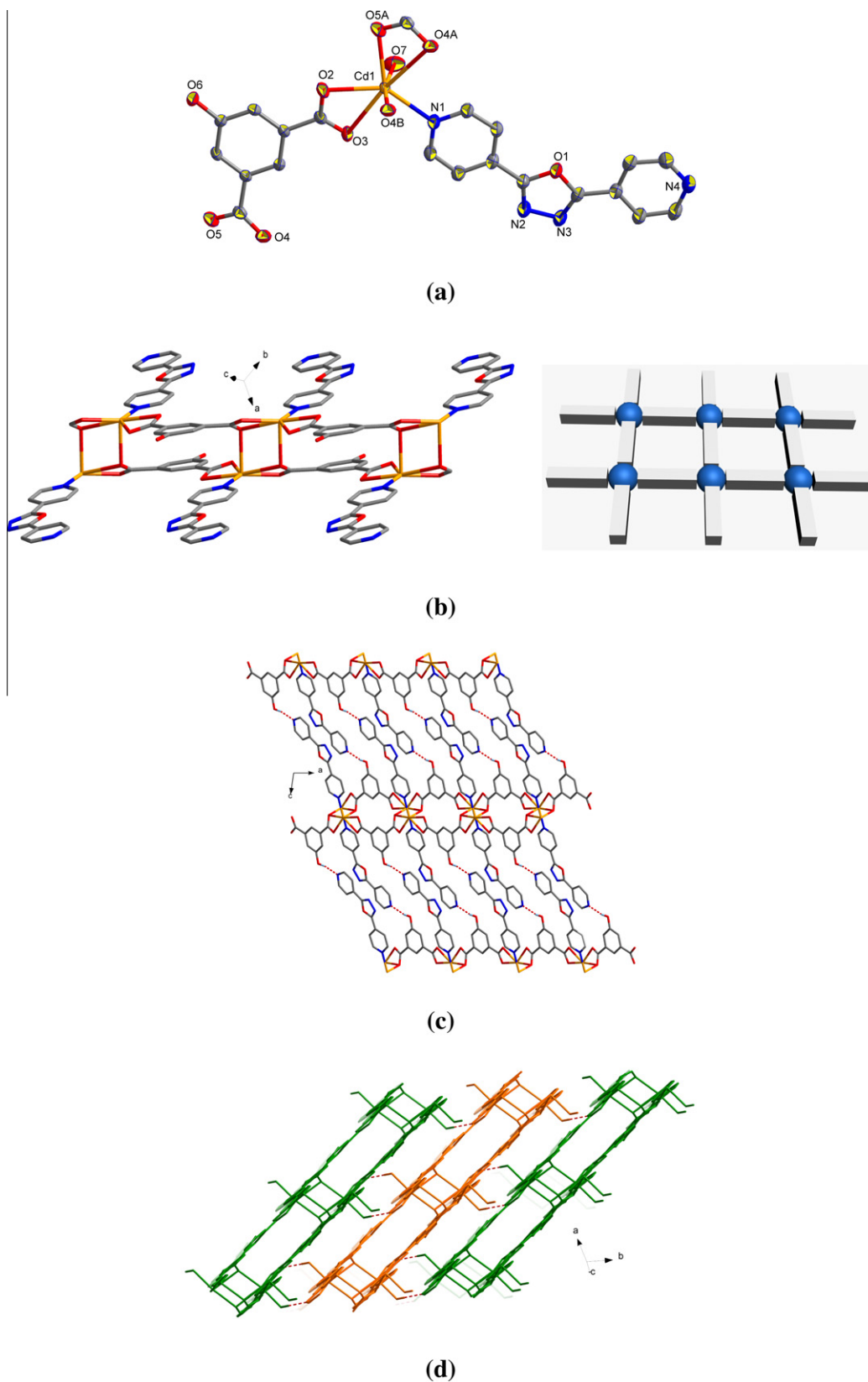


Fig. 2. Crystal structure of **2**. (a) A local view showing the coordination geometry of Cd^{II} (symmetry codes: $A = x + 1, y + 1, z$, $B = -x + 1, -y, -z + 1$). (b) Views of the 1-D dual-track coordination array. (c) 2-D hydrogen-bonding layer via interchain O–H...N interactions (shown as red dashed lines). (d) 3-D packing diagram highlighting the interlayer H-bonding interactions (shown as red broken lines). (For interpretation of the references to color in this figure legend, the reader is referred to the web version of this article.)

at 431 °C. No obvious decomposition is observed until heating to 600 °C and the residue holds a weight of 16.28%, corresponding

to that of ZnO (calculated: 16.68%). All the residual of metallic oxides were confirmed by PXRD (see Fig. S3).

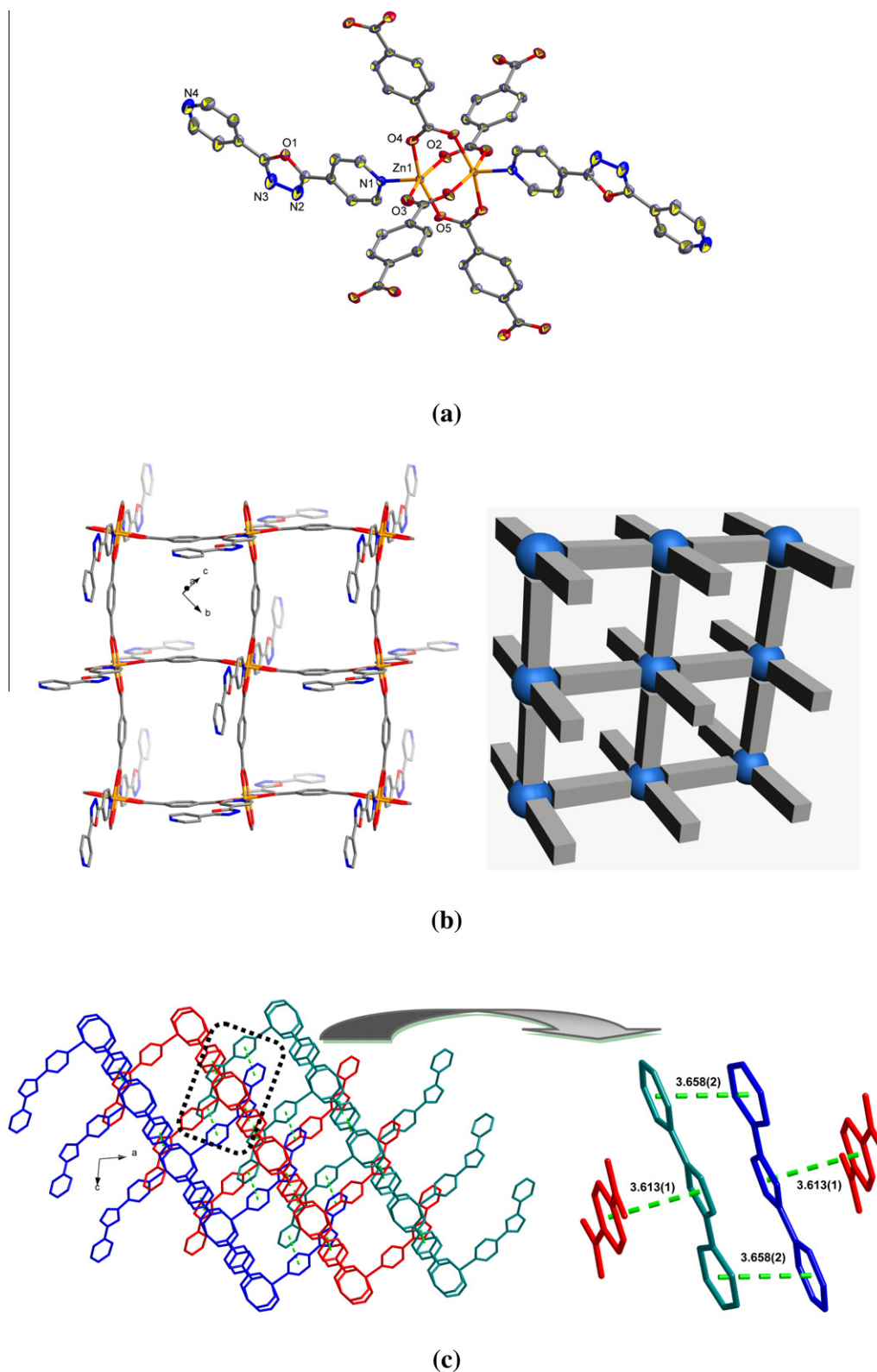


Fig. 3. Crystal structure of **3**. (a) A local view showing the coordination geometry of Zn^{II} . (b) Views of the 2-D coordination layer decorated with the terminal 4-bpo arms outside. (c) 3-D packing diagram highlighting the aromatic stacking interactions (shown as green broken lines). (For interpretation of the references to color in this figure legend, the reader is referred to the web version of this article.)

3.5. Fluorescence of complexes **1–3**

Notably, 1,3,4-oxadiazole system shows good electron affinity and electron-transmission ability for improvement of luminescent efficiency, which has been widely applied as the essential compo-

nent of photoluminescent, electroluminescent and non-linear optical materials [41]. Thus, solid-state fluorescent properties of complexes **1–3** were studied at room temperature to explore their potential for hybrid luminescent materials. Excitation of the Cd^{II} samples **1** and **2** at 350 nm leads to the maximum fluorescent

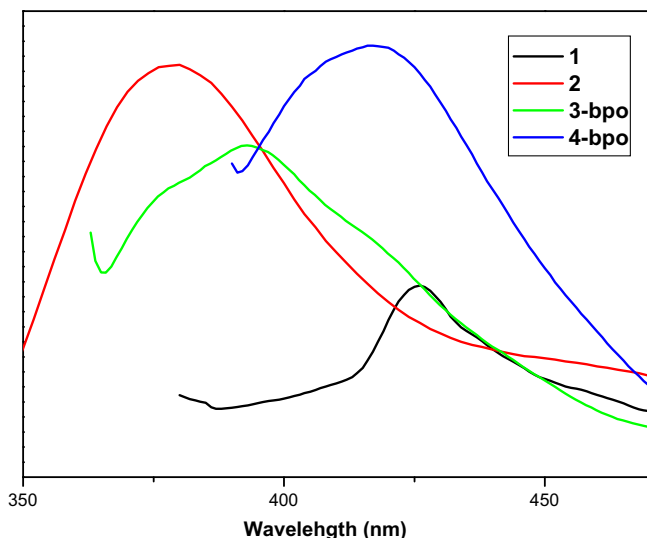


Fig. 4. Solid state fluorescent emissions of complexes **1** and **2**, as well as 3-bpo and 4-bpo ligands.

emission bands at 425 and 378 nm, respectively (see Fig. 4). However, no obvious emission is found for the Zn^{II} complex **3** under this excitation, which is probably due to the quenching effect of high-energy C–H and/or O–H oscillators from the CH₃OH solvent [42]. In addition, the maximal emissions of 3-bpo and 4-bpo ligands are observed at 393 and 417 nm ($\lambda_{\text{ex}} = 345$ and 370 nm). However for H₂mip or H₂hip ligand, no obvious emission peak is found under the similar conditions. Therefore, the emission peaks of Cd^{II} complexes should be ascribed to the intraligand $\pi \rightarrow \pi^*$ and/or $n \rightarrow \pi^*$ transitions with either 3-bpo or 4-bpo involved. Furthermore, the significant red-shift for **1** ($\Delta\lambda = 32$ nm) and blue-shift for **2** ($\Delta\lambda = 39$ nm) as well as the differences in luminescent intensity, compared with that of the corresponding free 3-bpo or 4-bpo ligand may be caused by the incorporation of metal–ligand coordination interactions. The fluorescent emission-shift phenomena are prevalently observed in the coordination complexes with 3-/4-bpo and benzenedicarboxylic acids [43–45].

4. Conclusion

This work presents three new Cd^{II} and Zn^{II} coordination polymers based on bent dipyriddy building blocks 3-/4-bpo and different benzenedicarboxylic acids under similar synthetic conditions. Apparently, their different network structures are largely dependent on the choice of metal ions and organic tectons, affording two 1-D Cd^{II} (tubular or dual-track motif) and one 2-D Zn^{II} (grid-like layer) coordination patterns, in which the 3-bpo and 4-bpo tectons exhibits the bidentate and unidentate coordination fashions, respectively, and all dicarboxylates act as the bridges to connect the metal centers. Additionally, diverse higher-dimensional supramolecular lattices are furnished via secondary interactions (H-bonding and aromatic stacking), which are also critical to stabilize the overall structures. Further efforts on such network-based metallosupramolecular assemblies with mixed ligands are underway.

Acknowledgment

This work was financially supported by Tianjin Normal University (No. 52X09004).

Appendix A. Supplementary material

CCDC 805649–805651 contain the supplementary crystallographic data for complexes **1–3**, respectively. These data can be obtained free of charge from The Cambridge Crystallographic Data Centre via www.ccdc.cam.ac.uk/data_request/cif. Supplementary data associated with this article can be found, in the online version, at doi:10.1016/j.ica.2011.08.069.

References

- [1] S.R. Batten, R. Robson, *Angew. Chem., Int. Ed.* 37 (1998) 1460.
- [2] J.J. Perry IV, J.A. Perman, M.J. Zaworotko, *Chem. Soc. Rev.* 38 (2009) 1400.
- [3] J.P. Zhang, X.C. Huang, X.M. Chen, *Chem. Soc. Rev.* 38 (2009) 2385.
- [4] J.S. Brooks, *Chem. Soc. Rev.* 39 (2010) 2667.
- [5] S.R. Batten, S.M. Neville, D.R. Turner, *Coordination Polymers: Design Analysis and Application*, RSC Publishing, 2009.
- [6] R.E. Morris, X. Bu, *Nature Chem* 2 (2010) 353.
- [7] S.L. James, *Chem. Soc. Rev.* 32 (2003) 276.
- [8] C. Janiak, *Dalton Trans.* (2003) 2781.
- [9] C.J. Kepert, *Chem. Commun.* (2006) 695.
- [10] X.Y. Wang, L. Wang, Z.M. Wang, S. Gao, *J. Am. Chem. Soc.* 128 (2006) 674.
- [11] L.F. Ma, L.Y. Wang, Y.Y. Wang, S.R. Batten, J.G. Wang, *Inorg. Chem.* 48 (2009) 915.
- [12] L.F. Ma, L.Y. Wang, M. Du, S.R. Batten, *Inorg. Chem.* 49 (2010) 365.
- [13] M.L. Zhang, D.S. Li, J.J. Wang, F. Fu, M. Du, K. Zou, X.M. Gao, *Dalton Trans.* (2009) 5355.
- [14] H.Y. Yang, L.K. Li, J. Wu, H.W. Hou, B. Xiao, Y.T. Fan, *Chem.-Eur. J.* 15 (2009) 4049.
- [15] S.M. Fang, Q. Zhang, M. Hu, X.G. Yang, L.M. Zhou, M. Du, C.S. Liu, *Cryst. Growth Des.* 10 (2010) 4773.
- [16] S.S. Chen, J. Fan, T. Okamura, M.S. Chen, Z. Su, W.Y. Sun, N. Ueyama, *Cryst. Growth Des.* 10 (2010) 812.
- [17] D. Maspoch, D. Ruiz-Molina, J. Veciana, *Chem. Soc. Rev.* 36 (2007) 770.
- [18] S. Sato, J. Tao, Y.Z. Zhang, *Angew. Chem., Int. Ed.* 46 (2007) 2152.
- [19] J.L.C. Rowsell, O.M. Yaghi, *Angew. Chem., Int. Ed.* 44 (2005) 4670.
- [20] M. Du, X.J. Zhao, J.H. Guo, S.R. Batten, *Chem. Commun.* (2005) 4836.
- [21] R.Q. Zou, H. Sakurai, Q. Xu, *Angew. Chem., Int. Ed.* 45 (2006) 2542.
- [22] Q.R. Fang, G.S. Zhu, Z. Jin, Y.Y. Ji, J.W. Ye, M. Xue, H. Yang, Y. Wang, S.L. Qiu, *Angew. Chem., Int. Ed.* 46 (2007) 6638.
- [23] Y.F. Zhou, M.C. Hong, X.T. Wu, *Chem. Commun.* (2006) 135.
- [24] Y.X. Hu, S.C. Xiang, W.W. Zhang, Z.X. Zhang, L. Wang, J.F. Bai, B.L. Chen, *Chem. Commun.* (2009) 7551.
- [25] W. Zhang, R.G. Xiong, S.D. Huang, *J. Am. Chem. Soc.* 130 (2008) 10468.
- [26] R.Q. Zou, A.I. Abdel-Fattah, H.W. Xu, Y.S. Zhao, D.D. Hickmott, *CrystEngComm* 12 (2010) 1337.
- [27] M. Du, Z.H. Zhang, L.F. Tang, X.G. Wang, X.J. Zhao, S.R. Batten, *Chem. Eur. J.* 13 (2007) 2578.
- [28] S.M. Fang, Q. Zhang, M. Hu, E.C. Sañudo, M. Du, C.S. Liu, *Inorg. Chem.* 49 (2010) 9617.
- [29] L.F. Ma, L.Y. Wang, J.L. Hu, Y.Y. Wang, G.P. Yang, *Cryst. Growth Des.* 9 (2009) 5334.
- [30] Z.G. Guo, R. Cao, X. Wang, H.F. Li, W.B. Yuan, G.J. Wang, H.H. Wu, J. Li, *J. Am. Chem. Soc.* 131 (2009) 6894.
- [31] R.Q. Zou, H. Sakurai, S. Han, R.Q. Zhong, Q. Xu, *J. Am. Chem. Soc.* 129 (2007) 8402.
- [32] F.A. Cotton, G. Wilkinson, C.A. Murillo, M. Bochmann, *Advanced Inorganic Chemistry*, sixth ed., John Wiley and Sons, New York, 1999.
- [33] M. Du, X.J. Jiang, X.J. Zhao, *Inorg. Chem.* 46 (2007) 3984.
- [34] X.L. Wang, C. Qin, E.B. Wang, *Cryst. Growth Des.* 6 (2006) 439.
- [35] M. Du, X.J. Jiang, X.J. Zhao, *Inorg. Chem.* 45 (2006) 3998.
- [36] M. Du, X.H. Bu, *Chem. Soc. Jpn.* 82 (2009) 539.
- [37] F. Bentiss, M. Lagrèe, *J. Heterocycl. Chem.* 36 (1999) 1029.
- [38] Bruker AXS, *SAINT Software Reference Manual*, Madison, WI, 1998.
- [39] G.M. Sheldrick, *SHELXTL NT Version 5.1. Program for Solution and Refinement of Crystal Structures*, University of Göttingen, Germany, 1997.
- [40] M. Du, Z.H. Zhang, X.G. Wang, L.F. Tang, X.J. Zhao, *CrystEngComm* 10 (2008) 1855.
- [41] A. Morsali, M.Y. Masoomi, *Coord. Chem. Rev.* 253 (2009) 1882.
- [42] B. Chen, Y. Yang, F. Zapata, G. Qian, Y. Luo, J. Zhang, E.B. Lobkovsky, *Inorg. Chem.* 45 (2006) 8882.
- [43] C.P. Li, J. Chen, M. Du, *CrystEngComm* 12 (2010) 4392.
- [44] C.P. Li, Q. Yu, J. Chen, M. Du, *Cryst. Growth Des.* 10 (2010) 2650.
- [45] J. Chen, C.P. Li, M. Du, *CrystEngComm* 13 (2011) 1885.